Journal of Photochemistry and Photobiology A: Chemistry 200 (2008) 262–269

Contents lists available at ScienceDirect

Journal of Photochemistry and Photobiology A: Chemistry

journal homepage: www.elsevier.com/locate/jphotochem

Photolysis of thin films of cypermethrin using in situ FTIR monitoring: Products, rates and quantum yields

Michal Segal-Rosenheimer, Yael Dubowski*

Faculty of Civil and Environmental Engineering, Technion—Israel Institute of Technology, Haifa 32000, Israel

ARTICLE INFO

Article history:
Received 26 June 2008
Received in revised form 31 July 2008
Accepted 2 August 2008
Available online 22 August 2008

Keywords:
Cypermethrin
Photolysis
Pesticides
Photooxidation

ABSTRACT

Cypermethrin is a synthetic pyrethroid insecticide commonly used both indoors and outdoors. Following its application, cypermethrin residues are exposed to atmospheric oxidants, such as ozone and OH radicals, as well as to solar radiation. The current work focuses on the photochemical degradation of cypermethrin under 254 nm, 310 nm, and solar radiation; including kinetic analysis, quantum yields, and identification of volatile and non-volatile products. The investigation was done using a combined FTIR set-up for parallel analysis of condensed and gas phases. Complementary GC–MS analysis was conducted on the pesticide's residues. Quantum yields of 0.41 and 0.25 were obtained under 254 and 310 nm, respectively. These values are in agreement with outdoor studies and are higher than the known yields for aqueous solution. The values obtained under all tested conditions suggest that photodegradation of adsorbed cypermethrin is a major outdoor degradation pathway. Oxygen presence was found to increase degradation rate and quantum yield.

The identified photoproducts include 3-phenoxybenzaldehyde, 3-phenoxybenzoic acid, acetonitrile (*m*-phenoxyphenyl), and cypermethrin isomers on the surface and formic acid, CO_2 and CO in the gas phase. The condensed phase products are more polar than the parent molecule, suggesting that they may be susceptible to a greater leaching rate in soils.

1. Introduction

α-Cypermethrin is a synthetic pyrethroid. It is less toxic when compared to other insecticides such as organophosphates, and hence, has been widely used both indoors and outdoors [1]. It is especially effective towards the control of insect pests in cotton, top fruits, vegetable crops, outdoor mosquito control and as an indoor insecticide [2].

Due to its low vapor pressure (1.3×10^{-9} mmHg at 20 °C), it is expected to be adsorbed upon aerosols and stagnant surfaces (e.g., soil, foliage, buildings etc.) that are exposed to atmospheric oxidants and solar radiation [3]. Atmospheric interactions are likely to have an important affect on the environmental fate of cypermethrin (and other pesticides), but still the present knowledge regarding these processes is lacking and only a few studies were carried out on the photolysis and atmospheric oxidation of sorbed cypermethrin [2,4–7]. Although these studies provide important information, the data available is still relatively sparse and is limited to mechanistic aspects and half-lives that depend on the specific illumination conditions used in these experiments. Furthermore, previously reported photochemical experiments were done under uncontrolled ambient atmosphere, and were therefore susceptible to the effect of atmospheric oxidants as well.

In a previous study conducted in our group, the oxidation of thin film of cypermethrin by gaseous ozone was investigated using FTIR spectroscopy and a novel apparatus allowing simultaneous monitoring of gaseous and condensed phases. The present investigation focuses on an additional degradation path of cypermethrin; the photochemical degradation of sorbed cypermethrin under controlled atmosphere and UV radiation. It provides, for the first time to the best of our knowledge, quantum yield values and real-time product analysis in both phases. Previously only CO_2 was suggested as a gaseous photoproduct [2,8]. Identification of gaseous products during cypermethrin photolysis can be of importance also for indoor air quality, considering the increasing use of short-UV radiation (254 nm) for the decomposition of air pollutants in indoor ventilation systems [9].

2. Experimental

2.1. Experimental set-up

Detailed description of the experimental system is given elsewhere [7]. In brief, the system consists of a 45° Horizontal ZnSe ATR

* Corresponding author. Tel.: +972 4 8295899; fax: +972 4 8228898.
E-mail addresses: Segalm@tx.technion.ac.il (M. Segal-Rosenheimer), yaeld@tx.technion.ac.il (Y. Dubowski).

1010-6030/$ – see front matter © 2008 Elsevier B.V. All rights reserved.
doi:10.1016/j.jphotochem.2008.08.004

crystal (HARTPlus, Pike Technologies, Inc.) placed in a flow-through homemade Stainless steal chamber with a quartz window at its top. Gas-phase species are detected downstream in a small volume long path IR cell (model 6.2 V, Infrared analysis, Inc.). ATR and IR cell are attached to separate FTIR spectrometers (Bruker Tensor 27 and Vertex 70, respectively) to allow simultaneous monitoring of both phases. A mercury lamp (model 3UV lamp-38, 8 watts UVP, Ltd.) was placed on top the quartz window, such that the film deposited on the ATR can be spectrally monitored while irradiated. The lamp had three illumination options centered at wavelengths of 254, 310 and 365 nm. It is important to note that these radiation sources are not monochromatic but rather emit in the following spectral ranges: 252–262, 280–386, and 340–417 nm, respectively.

2.2. Experimental procedures

The photodegradation was studied under the three different wavelengths and under three synthetic atmospheres: N_2 (>99.999% Maxima), dry mixture of N_2 and O_2 (>99.999% Maxima) at a ratio of 4:1, and similar N_2:O_2 mixture, but at high relative humidity conditions (RH = 80%). Humidification was obtained by bubbling the dry nitrogen gas through DI water (18.2 MΩ water, Millipore). RH and temperature of the gas flow were monitored in a mixing cell located just before the reactor's inlet, using AHLBORN Alemo® 2390-3 instrument. Cypermethrin film was deposited directly on the ATR crystal by applying 100 μl of 2 mM solution of α-cypermethrin (Riedel-de-Haën, analytical standard) in chloroform (BioLab, analytical reagent) and allowing the solvent to evaporate (complete removal of the solvent was confirmed by ATR spectra). The ATR flow-through chamber was then sealed to ambient atmosphere. Spectral measurements started simultaneously with the mounting of the UV lamp on top of the chamber's quartz window, while the proper gas mixtures were flowing continuously through it. Radiometric readings were taken using separate sensors, calibrated at 254, 310 and 365 nm (UVX Radiometers by UVP), that were mounted (in separate experiments) at the same location, distance and configuration as the ATR crystal in the experimental system. Irradiance measurements gave 0.45, 0.46, and 0.32 mW/cm^2, for the 254, 310, and 365 nm lamps, respectively.

The infrared absorbance spectra averaged 32 scans per spectrum at 2 cm^{-1} resolution for condensed phase and 1 cm^{-1} for the gas-phase analysis, over a spectral detection range of 4000–600 cm^{-1}. Background for the gas cell was taken under dry nitrogen flow, while clean ATR crystal served as background for the condensed phase spectra.

In addition to the laboratory studies, two qualitative photochemistry experiments were preceded under sunlight radiation. In each of these experiments a film of cypermethrin was similarly deposited on six carrier glasses. The carrier glasses were inserted into six quartz tubes with Teflon sealing flanges. Three pairs of different conditions were obtained as follows; two sealed tubes were covered with aluminum foil and served as controls, two tubes were filled with dry nitrogen and oxygen mixture (at a ratio of 4:1) and then sealed, and the last two tubes were left open to the ambient atmosphere.

Molar absorption coefficient of the cypermethrin film was determined by measuring its absorbance at varying concentrations. Films were deposited in a defined slot on a quartz slide, and their absorbance was measured between 200–500 nm (1 nm resolution) using UV–Vis spectrophotometer (Genesis 10 UV, Thermo®).

2.3. GC–MS analysis

The residue of the cypermethrin film was extracted at the end of the experiments with 3 ml of ethanol (BioLab, analytical reagent) and analyzed by GC–MS for the verification and identification of surface photoproducts. GC–MS analysis was performed on a CP-3800 Varian gas chromatograph with a capillary Column (VF5MS, 30 m, 0.25 mm ID, and film thickness of 0.25 um) attached to a Saturn 2000 mass spectrometer. Oven temperature was varied between 100 and 250 °C, using ramping rate of 10 °C/min. Injection port temperature was 270 °C with a split ratio of 1:10. Helium was used as the carrier gas.

3. Results

3.1. Spectral analysis of the condensed phase—kinetics and quantum yields

A detailed description of cypermethrin IR bands association was given previously [7]. The ATR–FTIR spectra recorded during the photolysis reaction of cypermethrin under 254 nm is shown in Fig. 1. As the exposure time increases, the absorbance at the bands associated with the ether-cyanate, the ester group (1125 and 1076 cm^{-1}, respectively), and with the terminal dihalogenvinyl group (920 cm^{-1}) decrease [7,10]. A decrease of the cypermethrin

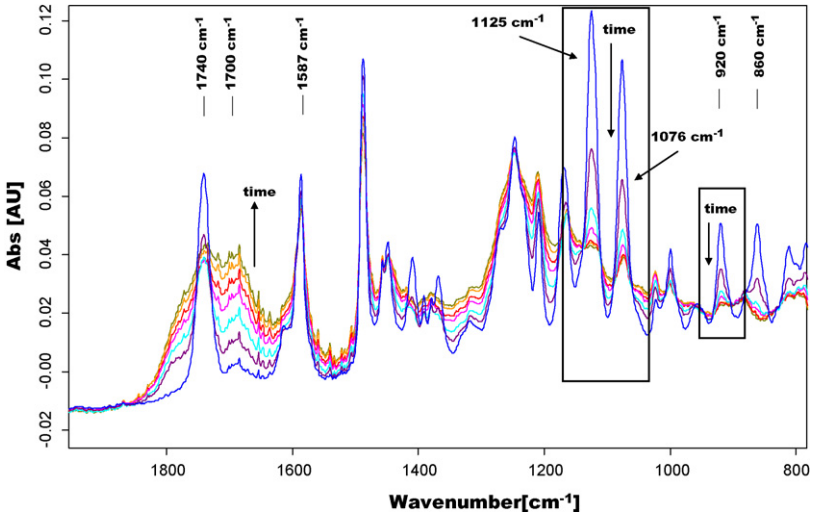

Fig. 1. ATR–FTIR spectra recorded during the photodegradation of cypermethrin under 254 nm radiation. Experiment was conducted under dry nitrogen and oxygen atmosphere. Time interval between lines is 20 min.

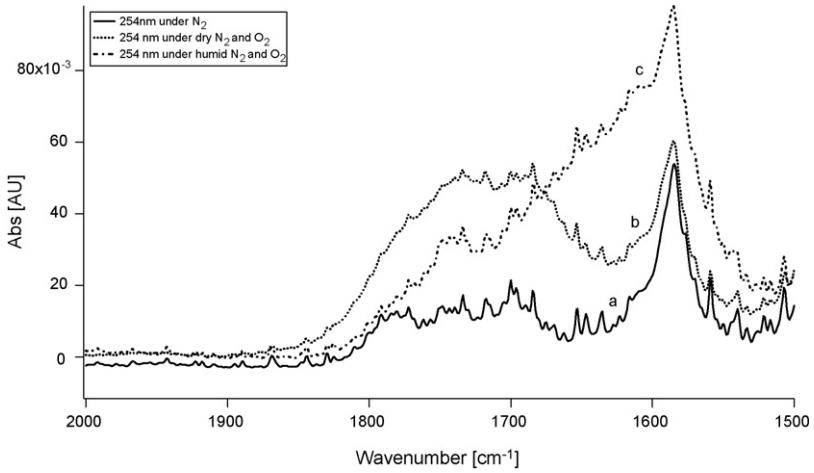

Fig. 2. IR spectra of cypermethrin film (between 1500 and 1800 cm^{-1}) after 2 h photolysis and removal of spectral contribution from the unreacted moeity (see text). Photolysis was done under 254 nm and (a) dry nitrogen atmosphere, (b) dry nitrogen and oxygen atmosphere, and (c) humid nitrogen and oxygen atmosphere.

carbonyl band (~1740 cm^{-1}) is also observed, in parallel to an increase of carbonyl signals adjacent to it: around 1650–1700 cm^{-1} and 1760–1780 cm^{-1}. As seen in Fig. 1, a shift is observed in the 860 cm^{-1} absorbance band (associated with the cyclopropane ring) [7,10].

The observed spectra are a superposition of both photoproducts and the parent material. The spectral contribution of the latter can be estimated based on the absorbance at 920 cm^{-1} band (which is unique to cypermethrin) [7], which can then be subtracted to yield the net spectra of the emerging products. Fig. 2 shows the results of such a subtraction done on spectra obtained after 2 h irradiation at 254 nm under the three tested "atmospheres", focusing on the 1500–1800 cm^{-1} range. As can be seen in Fig. 2, the presence of oxygen, both under dry and humid conditions, enhanced carbonyl formation. The main peaks increasing under the dry oxygenated atmosphere were at 1680–1700, 1740, and 1760 cm^{-1} while under humid conditions the main increase occurred around 1650 cm^{-1}. The bands at higher wavenumbers (1680 cm^{-1} and above) represent aldehyde and carboxylic acid carbonyl bands, while absorption at lower wavenumbers may be due to other products, such as acetonitrile (*m*-phenoxyphenyl).

3.1.1. Photolysis rate

The photolysis rate constants were extracted from the fit of temporal changes in absorbance peak area at the 920, 1076, 1125 and 1740 cm^{-1} bands. All the analyzed data fit an exponential decay model (p value <0.001), indicating first order kinetics. The experimental data under 310 nm showed similar spectral trends and product formation as was observed under the 254 nm radiation, but at slower rates. Under 365 nm radiation no significant spectral change was observed, indicating negligible degradation under this wavelength. Blank experiments of thin film cypermethrin under nitrogen and oxygen flows, excluding radiation, did not show any spectral change with time.

Under all tested atmospheres, photolysis rates under 254 nm irradiation were higher than under 310 nm, with averaged values of 0.036 and 0.0048 min^{-1}, respectively. Photolysis rates were enhanced under oxygenated atmosphere (both humid and dry). Similar trends were observed under both wavelengths but were more significant under 254 nm irradiation. (α value of 0.05 using ANOVA test).

Photolysis half-lives were calculated based on the decreasing absorbance in the 920 cm^{-1} band, which did not show any overlap with other absorbance bands and therefore was less susceptible to spectral artifacts. From the obtained first order photolysis rate constants k_p, half-lives could be determined:

$$t_{1/2} = \frac{\ln(2)}{k_p} \quad (1)$$

Calculated half-lives under 254 nm were 19, 15.5, and 16.5 min for dry nitrogen atmosphere, dry oxygenated atmosphere, and humid oxygenated atmosphere, respectively. These results are of the same order of magnitude as previously reported values [4]. Under 310 nm irradiation half-lives of 138, 114, and 144 min were calculated for dry nitrogen atmosphere, dry oxygenated atmosphere, and humid oxygenated atmosphere, respectively.

Unlike photodegradation rate constant and half-life values, which depend strongly on the experimental illuminescence intensity, obtaining quantum yields for these reactions will provide a better tool for comparison between experiments conducted at different laboratories and between laboratory and outdoor experiments.

3.1.2. Quantum yields

Quantum yield values for the reactions conducted were calculated based on the following equation;

$$\Phi = \left(\frac{dC/dt}{dI_{abs}/dt}\right) \quad (2)$$

where dC/dt is the observed initial photodegradation rate, and dI_{abs}/dt is the light flux absorbed by the cypermethrin film.

The absorbed light (I_{abs}) is a function of both the incident light flux (I_0) and the average molar absorption coefficient $<\varepsilon>$. I_0 was calculated based on the light flux measured using the specific radiometers for each lamp and a correction factor compensating for the differences between spectral illumination curves of the UV lamps (or the sun) and the spectral responsivity curves of the corresponding radiometers (detailed explanation is provided in Appendix A).

$<\varepsilon>$ was calculated over the spectral range of the radiometers (λ_1 to λ_2) according to

$$\langle\varepsilon\rangle = \frac{\int_{\lambda_1}^{\lambda_2} I(\lambda)\,\varepsilon(\lambda)\,d\lambda}{\int_{\lambda_1}^{\lambda_2} I(\lambda)\,d\lambda} \quad (3)$$

where $I(\lambda)$ represents the lamp spectral output function and $\varepsilon(\lambda)$ is the measured molar absorptivity of cypermethrin film at wavelength λ. Since the film thickness is estimated to be less than 40 nm,

Table 1
Quantum yield values for photolysis of cypermethrin thin film under 254 and 310 nm radiation[a]

Experimental conditions	254 nm	310 nm
Dry N_2 atmosphere	0.37 ± 0.03 (5)	0.23 ± 0.03 (3)
Dry N_2 and O_2 atmosphere	0.46 ± 0.07 (7)	0.28 ± 0.05 (5)
Humid N_2 and O_2 atmosphere	0.42 ± 0.04 (5)	0.22 ± 0.05 (5)

[a] Values in parenthesis refer to the number of experiments made under each condition.

as we have previously shown for similar films [7], diffused reflectivity of the film can be neglected in this wavelength range (>254 nm), according to the Rayleigh criterion [11].

Following the above, the actual light flux initially absorbed by the cypermethrin film (I_{abs}) is given by

$$I_{abs} = I_0 \times \langle \varepsilon \rangle \times [C]_0 \quad (4)$$

where $[C]_0$ is the initial cypermethin thin film surface concentration in molecules/cm^2.

Table 1 summarizes the quantum yield values obtained for the photodegradation of thin film cypermethrin on a ZnSe surface under the different experimental conditions. As shown, under both 254 and 310 nm irradiations, the quantum yields under oxygenated conditions were higher. The quantum yields obtained under 254 nm radiation were significantly higher than those under 310 nm radiation, as expected.

As was mentioned earlier, in order to confirm our experimental quantum yield for 310 nm radiation, additional photolysis experiments of cypermethrin were performed under sunlight radiation. Such comparison is valid assuming that cypermethrin quantum yield does not vary significantly over the range of 280–305 nm.

In the outdoor photolysis experiments cypermethrin thin film samples under synthetic atmosphere of dry nitrogen and oxygen (4:1 mixing ratio) showed 70% degradation after 4 days.

Table 2
Products formation yields (in percentage relative to reacted cypermethrin) during photochemical reaction of cypermethrin under sunlight radiation

Retention time (min)	Compound name	Molar fraction before reaction	Molar yield after reaction under controlled atmosphere	Molar yield after reaction under uncontrolled atmosphere
10.768	3-PB-aldehyde	2.5	22	41
12.69	ACN-P	0	1.9	2.9
12.9	3-PB-acid	0.5	0.45	3.4
23.503	Cyper—isomer 1[a]	3.5	0	0
24.041	Cyper—isomer 2[a]	93.5	40	11.3
24.18	Cyper—isomer 3[a]	0	12.65	8.3
Total		100%	77%	67%

[a] All three isomers were identified by the instrument's library search algorithm as cypermethrin (over 98% certainty).

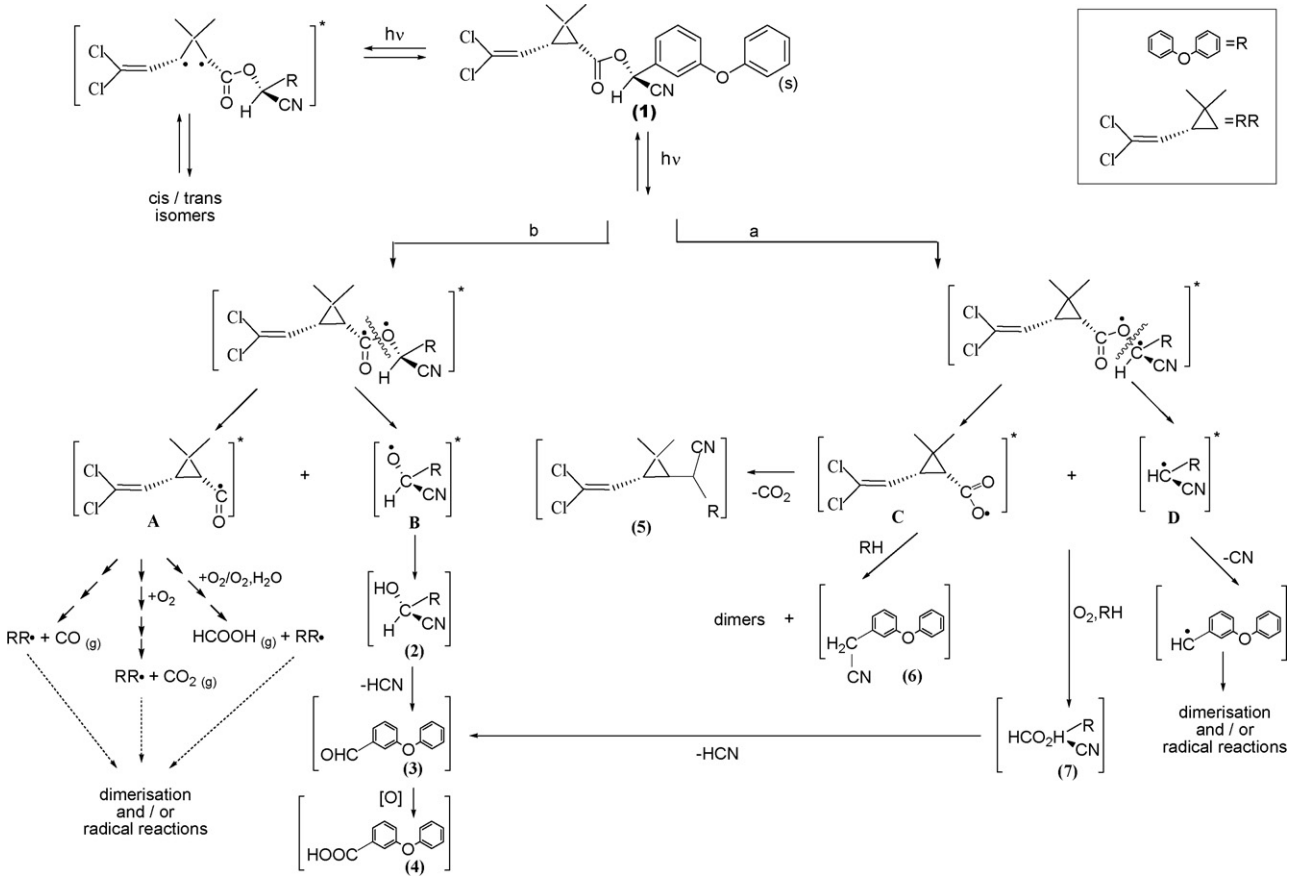

Scheme 1. Suggested mechanism for the photolysis reaction of cypermethrin.

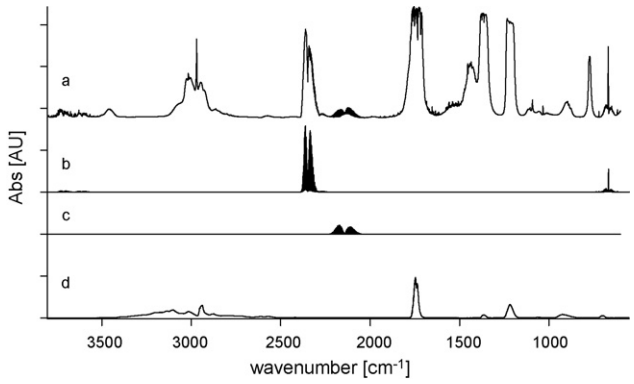

Fig. 3. LP–IR cell spectra of the gas phase (a) composite spectrum after the photolysis reaction under 254 nm radiation, (b) CO_2 spectrum, (c) CO spectrum, and (d) formic acid spectrum. Reference spectra were taken from PNNL spectral gas-phase database. Spectra are shifted for clarity.

3.2. Spectroscopic and chromatographic product analyses

3.2.1. Condensed phase products

Product identification of the condensed phase was conducted using both gas chromatography and spectral analysis methods. GC–MS analysis revealed the following products (Table 2); 3-phenoxybenzaldehyde (3-PB-aldehyde, product no. 3 in Scheme 1), 3-phenoxybenzoic acid (3-PB-acid, product no. 4 in Scheme 1), Acetonitrile (*m*-phenoxyphenyl) (ACN-P, product no. 6 in Scheme 1), and an additional cypermethrin isomer (i.e., isomer 3). Quantification of the identified photoproducts was possible using commercial standards for GC calibration. Such analysis was carried out for cypermethrin films that were exposed to solar radiation under synthetic dry atmosphere (N_2:O_2 = 4:1) and under open ambient atmosphere. Products formation yields were estimated by dividing the amount of the generated product by the amount of consumed cypermethrin and are shown in Table 2 (Cypermethrin was calibrated according to the isomer emerging at 24.04 min and an assumption on similarity was made for the other two isomers).

3.2.2. Gas-phase products

Gaseous products were detected using a mini-LP IR cell located downstream of the photochemical reactor. Due to low concentrations under flow-through conditions, gas phase products were identified under separate experiments, in which reaction took place inside the sealed cell attached to the ATR. At the end of the photochemical experiment, the head space was flushed downstream to the pre-pumped LP IR cell. Fig. 3a shows the gaseous phase spectra of the emerging products observed during the photolysis reaction under 254 nm radiation and dry atmosphere of nitrogen and oxygen. Among the gaseous products, CO_2 and CO are clearly identified (Fig. 3b and c, respectively). Formic acid fits well with the additional spectral bands at 1100, 1200, 1735 and around 3000 cm^{-1} (Fig. 3d). However, these three products cannot account for the absorbance bands at 778, 1435, and 1460 cm^{-1}, indicating the presence of additional gaseous photoproducts. Gas-phase products under 310 nm radiation showed the same peaks but with significantly lower signals.

4. Discussion

Under UV radiation, the ether or the ester bonds of cypermethrin are expected to break and split the molecule [6], as shown in Scheme 1. Indeed, the absorbance bands associated with these functional groups (1076 and 1125 cm^{-1}) show a decrease upon irradiation (Fig. 1). The observed loss rates of these bands were proven to be statistically similar, suggesting that both pathways of ether cleavage and ester cleavage degradation (Scheme 1) are similar in their occurrence rate.

4.1. Photolysis rate and quantum yields

The photolysis rates obtained from the ATR data are in agreement with previous reported values for adsorbed cypermethrin on glass surface under 254 nm irradiation [4]. Regarding photolysis under solar radiation, our outdoor experiment implies a half-life of 22–29 light hours (considering about 10 h of light a day during the experiment time at the beginning of July and assuming an exponential decay process). This value is in good agreement with previously reported half-life values for outdoor photolysis of cypermethrin adsorbed on soils (0.6–1.9 days by Takahashi et al. and 2.2 and 3.2 days by Raikwar and Nag) [2,4], despite the differences in these surfaces properties.

The present laboratory experiments show that the photolysis rates of cypermethrin are enhanced under oxygenated atmosphere. It is possible that oxygen accelerates the reaction by promoting the stabilization of intermediate products (e.g., product D in Scheme 1) [6] or by participating in radical formation (pathway 'b' in Scheme 1). Relative humidity was also found to enhance the reaction rate supporting the assumption that it is also an active participates in the reaction mechanism (as shown in Scheme 1).

Quantum yield is an essential parameter for quantitative comparison between results from different experiments. Unfortunately, quantum yields for cypermethrin photolysis were previously reported only for the cis and trans isomers in aqueous solutions under sunlight (0.16 and 0.097, respectively) [2]. These values are about a factor of 2 lower than the quantum yields obtained in the present study for cypermethrin film under 310 nm irradiation. Nevertheless, this trend (i.e., higher yield for cypermethrin photodegradation on surfaces than in solution) is in agreement with the 1.7-times higher loss rates measured for cypermethrin film on soils relative to aqueous solutions [2]. Furthermore, based on the quantum yield obtained in the present laboratory study (0.25 under 310 nm irradiation) and the solar irradiance in our geographical location, a photodegradation rate and half-life can be calculated. The half-life calculated this way, using tabulated solar irradiance data [12] for a solar zenith angle of 10° (corresponding to mid-summer zenith angle at our location, 32°N, at mid-day) is of the order of 19 h. This value is in good agreement with the observed outdoor experimental results.

Under open atmospheric conditions, cypermethrin degradation was more rapid, yielding more 3-PB-aldehyde and probably more gas phase products. This may suggest the participation of other atmospheric oxidants, such as O_3 and OH radicals, under ambient atmospheric conditions.

4.2. Surface products

The observed spectral changes in the carbonyl region (1680-1780 cm^{-1}) suggest the formation of carbonyl groups such as aldehydes and carboxylic acids, which differ from the reactant's initial carbonyl group. The shift in the 860 cm^{-1} band supports the isomerization of cypermethrin, which is known to occur during its photochemical degradation [6] and is also supported by our GC–MS product analysis.

GC–MS analysis of the cypermethrin residue indicated that the main photoproducts are 3-PB-aldehyde and the cypermethrin isomer (Table 2). The formed isomer (#3, emerging at 24.18 min and identified by the GC–MS algorithm as cypermethrin), is suspected to be the trans isomer, as was previously suggested for aqueous solution systems [2,6]. ACN-P was found to be a minor product and

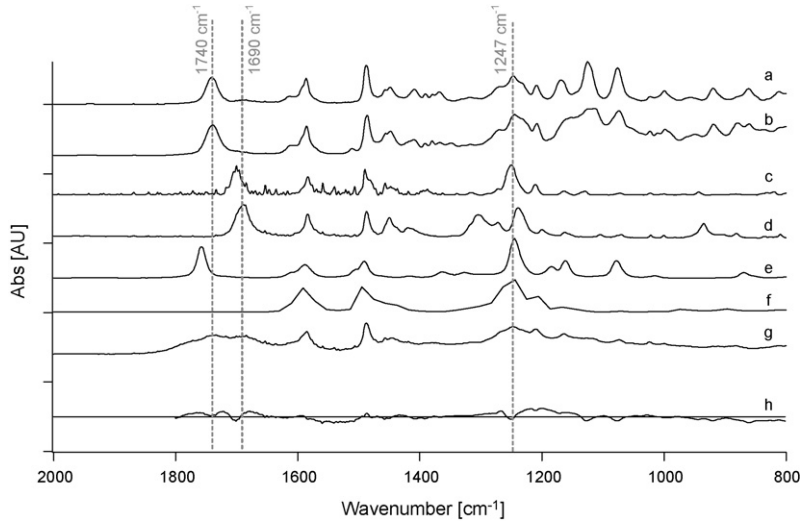

Fig. 4. ATR–FTIR spectra of the condensed phase of (a) cypermethrin film (standard grade) before reaction, (b) cypermethrin film (mixed isomer grade) (c) 3-PB-aldehyde, (d) 3-phenoxybenzoic acid, (e) 4-phenoxybenzoic acid, (f) acetonitrile (*m*-phenoxyphenyl), (g) cypermethrin film after photochemical reaction under 254 nm radiation and dry nitrogen and oxygen atmosphere, and (h) reconstructed spectrum error based on inverse calculations, as detailed in text. Absorbance units were scaled arbitrarily and hence are not quantitative. Spectrum h is one order of magnitude smaller than upper spectra.

the obtained low yields of 3-PB-acid are very likely the result of our low sensitivity to carboxylic acids as no dervitization was used. The obtained yields and incomplete molar balance may indicate the formation of additional unidentified products or gaseous products.

Fig. 4 shows the spectra of the different identified condensed phase products, in comparison with the spectra of the film residue at the end of reaction. As shown, 3-PB-aldehyde and the 3-phenoxybenzoic acid (spectra b and c) can explain much of the broadening and increase at the spectral range between 1650 and 1720 cm^{-1}. Also, the cypermethrin film of mixed isomers is shown to be contributing to the spectral change around 860 cm^{-1}, as suggested earlier. The increase in the band of 1760 cm^{-1} is associated with 4-phenoxybenzoic acid (4-PBA acid), which unfortunately cannot account for all of the changes occurring above the 1740 carbonyl band. It is possible that additional products are present, as found by Takahashi et al. and Raikwar and Nag [2,4], but were not identified by us. Also seen is the contribution of the ACN-P at the 1200 and 1600 cm^{-1} bands. Although the latter can explain well the spectral changes around those regions, it cannot, quantitively, be accounted for all of it. Following the above, the identified products cannot be the sole contributors of the observed spectral change, in agreement with the incomplete molar balance shown in Table 2. Nevertheless, as we will show below, the identified products can explain most of the spectral change during reaction.

A first approximation of the products' relative contribution to the film's spectra during reaction can be deduced, assuming that at each time point the observed spectrum is a linear combination of the pure reactant and products' spectra (i.e., end-members spectra) and applying a spectral inverse model (see Appendix B). Hence, the acquired absorbance spectra can be described by the following matrix notation:

$$[A] = [E] \times [f] \quad (5)$$

where $[A]$, $[E]$, and $[f]$ are matrixes with the following dimensions; $[m \times t]$, $[m \times n]$, and $[n \times t]$, respectively, with m being the number of wavenumbers, n the number of end-members, and t the number of spectrums acquired during a whole experiment. As $[A]$, the recorded spectra matrix, and $[E]$, the end-members spectra, are known, the fractions of each component at a specific time t can be calculated using matrix division.

This spectral inverse modeling was done on the observed spectra of the different experiments. Calculations have shown that the major contributors to the spectral changes were the 3-PB-aldehyde and the cypermethrin isomers (shown in Fig. 4b and c). All other products contributed a small change to the spectral reconstruction and to the spectral reconstruction error. The spectral reconstruction error was calculated from the subtraction of the calculated reconstructed spectrum from the corresponding measured spectrum. Calculations were done only within the fingerprint spectral region between 800 and 1800 cm^{-1}. One representing example is shown in Fig. 4h. The major deviations were around 1200 and 1700 cm^{-1}, and the maximal reconstruction error was under 10% from the original spectra in all experiments. Positive deviations may be contributed by additional unidentified products (e.g., dimer's absorbance around 1200 cm^{-1}), and the negative peak around 1700 cm^{-1} may suggest a small overestimation of the produced 3-PB-aldehyde.

In addition, the calculated temporal relative fractions of each component could give an estimation of the reaction progress and rate. A good agreement was obtained between the rates estimated using the inverse method and those calculated based on the 920 cm^{-1} peak decrease (deviations of up to 0.005 min^{-1} in reaction rate constants relative to the obtained experimental rates).

4.3. Suggested photolysis mechanism

In general, following its excitation under direct photolysis, cypermethrin can follow three primary paths resulting in the formation of cis/trans isomerization or degradation via ester or ether-cyanate cleavages (Scheme 1).

The observed surface products and the decrease in ether-cyanate absorbance band (1125 cm^{-1}) are in agreement with previously proposed photolysis mechanisms of cypermethrin [6] presented as path 'a' in Scheme 1. Nevertheless, no species including cyclopropane derivatives were observed, in agreement with our incomplete mass balance and spectral analysis discussed above. In parallel to the breakage of the ether-cyanate group, our ATR spectra shows a simultaneous decrease of the 1076 cm^{-1} band (C═O)–O–, indicating an ester cleavage (path b in Scheme 1), as also reported by Raikwar and Nag [4]. Such ester cleavage will lead to the formation of two unstable intermediates (A and B).

Under oxygenated atmospheric conditions, intermediate A was postulated to yield CO, CO_2 and formic acid, which indeed were detected in the gas-phase. The chlorinated cyclopropane radical that is expected to be formed on the surface (product RR•), is known to recombine to form dimers, [4] or higher molecular weight products. Such products, although not detected by our GC–MS analysis, may be supported by the broad absorbance increase between 1100 and 1300 cm^{-1}, as shown in Fig. 1. The chlorinated radical might also participate in other radical chain reactions or be subjected to hydrogen abstraction reaction and breakage of its double bond. The main observed degradation products, 3-PB-aldehyde (product 3) and 3-PB-acid (product 4), can be derived from intermediates B and D under oxygenated conditions, in agreement with the reduced formation of these carbonyl species under pure N_2 atmosphere (Fig. 2a). The formation of product 6 (ACN-P) was previously suggested to depend on relative humidity [6]. The present results, showing stronger absorbance around the 1600 cm^{-1} under humid conditions (Fig. 2c), support this path. Product 7 was not observed in the current study, which is not surprising considering it is known to readily convert [6] into products 3 or 4. Similar to the behavior of the chlorinated radical (RR•), the phenoxy radical, generated in pathway 'a' can further react to form dimers or participate in different radical reactions that can attack the double bond.

4.4. Environmental implications

During application, cypermethrin is usually sprayed as a mixture of organic solvents that rapidly evaporate, leaving the active ingredient airborne or deposited [13,14] on different surfaces that are continuously exposed to the atmosphere and solar radiation. Both measured and calculated half-lives of cypermethrin under solar radiation were about 20 h, indicating that photochemical degradation is one of the most important pathways of this material outdoors. Previous studies have shown that even for low-volatility pesticides, significant portions of the applied material can reach non-target areas via atmospheric transport [15]. The quantum yields obtained in the present study and the lifetime of atmospheric aerosols [16], suggest that non-target areas located even few kilometers down wind from applied fields are likely to be exposed to a mixture of cypermethrin isomers and its degradation products. The agreement between calculated quantum yields under laboratory 310 nm lamp, and the observed outdoor loss rate under solar radiation, support the possibility to use quantitative laboratory data to estimate atmospheric photodegradation.

The detected gaseous products: carbon dioxide, carbon monoxide, and formic acid are likely to quickly disperse outdoors without posing significant health problem. In the indoor environment these gaseous products might form when 254 nm light is used for decontamination in ventilation systems, nevertheless the levels produced are not likely to pose a health problem.

The condensed phase products: 3-phenoxybenzaldehyde, 3-phenoxybenzoic acid, and acetonitrile *m*-phenoxyphenyl are more polar than the parent molecule and may be susceptible to a greater leaching rate in soils, [1] resulting in a greater groundwater contamination probability. Furthermore, the major photoproduct observed, 3-PB-aldehyde, is a toxic compounds that was recently proven to have estrogenic activity [17].

Comparing the effects of atmospheric ozone [7] and solar radiation on the fate of adsorbed cypermethrin suggest that under ambient conditions photolysis is faster and possibly a major outdoor degradation pathway, while indoors ozonolysis is likely to be important. Despite the different mechanisms, the resulting surface products of both processes were quite similar. With respect to gaseous products, more variability was found, with phosgene being detected only during ozonolysis and formic acid only during photolysis.

Acknowledgment

This research was funded by Marie Currie International Reintegration grant, as part of the sixth framework programme of the European Commission.

Appendix A. Correction of measured radiant flux

Since the spectral illumination curves of the UV lamps (or the sun) do not perfectly overlap with the spectral responsivity curves of the corresponding radiometers, as shown in Fig. A.1, the measured flux had to be adjusted by a correction factor as follows:

$$I_0 = I_{\text{measures}} \times \text{CF} \tag{A1}$$

$$\text{CF} = \frac{\int_{\lambda_1}^{\lambda_2} I(\lambda)\ \mathrm{d}\lambda}{\int_{\lambda_1}^{\lambda_2} I(\lambda) r(\lambda)\, \mathrm{d}\lambda} \tag{A2}$$

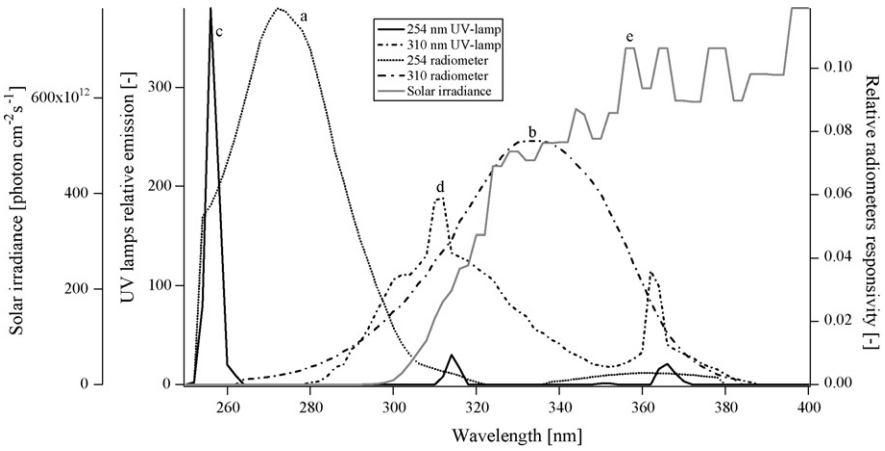

Fig. A.1. Relative spectral responsivity curves of (a) 254 nm radiometer, (b) 310 nm radiometer, and the spectral illumination curves of (c) 254 UV lamp, (d) 310 UV lamp used in the laboratory experiments, and (e) solar UV spectrum taken from tabulated irradiance data for a solar zenith angle of 10° (Finlayson–Pitts and Pitts, 2000). UV lamps and radiometer responsivity curves are given in relative units.

where λ_1 and λ_2 are the lower and upper boundaries of the wavelength range at which the measurements were taken (i.e., the radiometer range), $I(\lambda)$ is the lamp spectral output function and $r(\lambda)$ is the radiometer response normalized to its calibration wavelength.

Appendix B. Inverse method calculations

A first approximation of the products' relative amounts in the composite spectra during reaction was deduced, assuming that at each time point the observed spectrum is a linear combination of the pure reactant and products' spectra (i.e., end-members spectra) Hence, each absorbance spectrum at time t can be described by the following set of linear equations:

$$\begin{aligned} A_1 &= e_{11}f_1 + e_{12}f_2 + \cdots + e_{1n}f_n \\ A_2 &= e_{21}f_1 + e_{22}f_2 + \cdots + e_{2n}f_n \\ &\vdots \\ A_m &= e_{m1}f_1 + e_{m2}f_2 + \cdots + e_{mn}f_n \end{aligned} \tag{B1}$$

where A_i is the IR absorbance reading at a specific wavenumber i (given for m wavenumbers) for a specific spectrum in time, e_{ij} is the jth end-member signal (where there are n end-members) at the specific wavenumber i, and f_j is the fraction of the jth end-member at that specific temporal spectrum. Using the shortened vector form we receive:

$$\vec{A} = [E] \times \vec{f} \tag{B2}$$

where $\vec{A}$ is the absorbance vector at time t with the dimensions of $[m \times 1]$, $[E]$ is the end-member matrix with the dimensions of $[m \times n]$, and $\vec{f}$ is the end-member's fraction vector with the dimensions $[\mathrm{n} \times 1]$. As we have t spectra, one for each acquisition in time, the full set of linear equations can be described by the following notation;

$$[A] = [E] \times [f] \tag{B3}$$

where, $[A]$, $[E]$, and $[f]$ are matrixes with the following dimensions; $[m \times t]$, $[m \times n]$, and $[n \times t]$, respectively. t is the number of spectrums acquired during a whole experiment. As $[A]$, the recorded spectra matrix, and $[E]$, the end-members spectra, are known, the fractions of each component at a specific time t can be calculated simultaneously using following equation:

$$[f] = \mathrm{INV}[E] \times [A] \tag{B4}$$

where INV$[E]$ is the inverse matrix of $[E]$.

References

[1] D.D. Kaufman, B.A. Russell, C.S. Hellingand, A.J. Kayser, Movement of cypermethrin, decamethrin, permethrin, and their degradation products in soil, Journal of Agricultural and Food Chemistry. 29 (1981) 239–245.

[2] N. Takahashi, N. Mikami, T. Matsuda, J. Miyamoto, Photodegradation of the pyrethroid insecticide cypermethrin in water and on soil surface, Journal of Pesticide Science 10 (1985) 629–642.

[3] E. Bacci, D. Calamari, C. Gaggiand, M. Vighi, An approach for the prediction of environmental distribution and fate of cypermethrin, Chemosphere 16 (1987) 1373–1380.

[4] M.K. Raikwar, S.K. Nag, Phototransformation of alphacypermethrin as thin film on glass and soil surface, Journal of Environmental Science and Health, Part B: Pesticides Food Contaminants and Agricultural Wastes 41 (2006) 973–988.

[5] L.O. Ruzo, E.C. Kimmel, J.E. Casida, Ozonides and epoxides from ozonization of pyrethroids, Journal of Agricultural and Food Chemistry 34 (1986) 937–940.

[6] L.O. Ruzo, V.V. Krishnamurthy, J.E. Casida, K. Gohre, Pyrethroid photochemistry—influence of the chloro(trifluoromethyl)vinyl substituent in cyhalothrin, Journal of Agricultural and Food Chemistry 35 (1987) 879–883.

[7] M. Segal-Rosenheimer, Y. Dubowski, Heterogeneous ozonolysis of cypermethrin using real-time monitoring FTIR techniques, Journal of Physical Chemistry C 111 (2007) 11682–11691.

[8] T. Katagi, Photodegradation of the pyrethroid insecticide esfenvalerate on soil, clay–minerals, and humic-acid surfaces, Journal of Agricultural and Food Chemistry 39 (1991) 1351–1356.

[9] A.I. Hodgson, H. Destaillats, D.P. Sullivan, W.J. Fisk, Performance of ultraviolet photocatalytic oxidation for indoor air cleaning applications, Indoor Air 17 (2007) 305–316.

[10] D. Lin-Vien, Colthup N B., W.G. Fateley, J.G. Grasselli, The Handbook of Infrared and Raman Frequency of Organic Molecules, Academic Press, 1991.

[11] C.F. Bohren, D.R. Huffman, Absorption and Scattering of Light by Small Particles, John Wiley and sons, Inc, 1983, pp. 36–41.

[12] B.J. Finlayson-Pitts, J.N. Pitts, Chemistry of the Lower and Upper Atmosphere, Academic Press, 2000.

[13] F. Ferrari, M. Trevisan, E. Capri, Predicting and measuring environmental concentration of pesticides in air after soil application, Journal of Environmental Quality 32 (2003) 1623–1633.

[14] F. Van den Berg, R. Kubiak, W.G. Benjey, M.S. Majewski, S.R. Yates, G.L. Reeves, J.H. Smelt, A.M.A. van der Linden, Emission of pesticides into the air, Water Air and Soil Pollution 115 (1999) 195–218.

[15] J.N. Seiber, M.M. McChesney, J. E. Woodrow, Experimental validation of model-predicted volatilization rates of pesticides from water, Abstracts of Papers of the American Chemical Society, 1985, 190 (1985-99-AGO).

[16] H. de-ruiter, H.J. Holterman, C. Kempenaar, H.J.L. Mol, J.J. de Vlieger, J.C.V. de Zande, Influence of adjuvants and formulations on the emission of pesticides to the atmosphere, Plant Research International B.V. (2003).

[17] A.R. McCarthy, B.M. Thomson, I.C. Shaw, A.D. Abell, Estrogenicity of pyrethroid insecticide metabolites, Journal of Environmental Monitoring 8 (2006) 197–202.